Study of the Powerful Nd:YLF Laser Amplifiers for the CTF3 Photoinjectors

Massimo Petrarca, Mikhail Martyanov, Marta "Csatari" Divall, and Grigory Luchinin

***Abstract*— A high-power neodymium-doped yttrium lithium fluoride (Nd:YLF) mode-locked 1.5-GHz laser currently used to drive the two photoinjectors of the Compact Linear Collider Test Facility project at the European Organization for Nuclear Research is described. A phenomenological characterization of the two powerful Nd:YLF amplifiers is presented and compared with the measurements. The laser system operates in a saturated steady-state mode. This mode provides good shot-to-shot stability with pulse train mean power in the 10 kW range.**

***Index Terms*— Diode pump, Nd:YLF amplifier, photoinjector laser, saturated steady-state.**

I. Introduction

THE main task of the Compact Linear Collider Test Facility (CTF3) at the European Organization for Nuclear Research (CERN) is to demonstrate the feasibility of the key compact linear collider (CLIC) technology challenges for the CLIC two-beam scheme, i.e., acceleration of the main electron beam using the RF power emitted from strong deceleration of the second beam, referred to as a drive beam [1]–[3].

The drive beam is currently produced by a thermionic gun followed by a bunching system that transforms continuous electron current into well-localized electron bunches. This, however, introduces unwanted satellite bunches.

For the drive and main beam, laser-driven photoinjectors have been developed. The PHotoINjector (PHIN) and Concept d'Accélérateurs Linéaire pour Faisceau Sonde (CALIFES) projects, respectively, were dedicated to attain the photoinjector parameters and to study their long-term reliability.

A photoinjector is an attractive alternative [4] to generate electron bunches directly with the right time structure from a laser where electrons are produced through the photoemission process using, in our case, Cs_2Te photocathodes. Another advantage of a photoinjector is that the high-gradient RF accelerating field of the gun and a high-quality laser beam together produce low-emittance electron beams, i.e., beams with small transverse size and divergence [5], [6].

The laser pulse duration corresponds to the required electron bunch length, and a mode-locked pulse train together with fiber-optic modulators and fast Pockels cells ensures the structure required for the CTF3 project [3], [7] (Table I). However, to provide a stable electron source for the future CLIC machine, PHIN needs to demonstrate a very low electron bunch charge fluctuation (<0.1% rms) [8]–[10], which demands very high laser amplitude stability. Saturated steady-state (SSS) amplification has been chosen as a mode of operation to support these tight requirements [11], [12].

The photoinjector laser provides a unique pulse structure determined by the machine application. Similar laser systems have been developed for DESY [13] with a lower mode-locked repetition rate (RR) but similar power characteristics using neodymium-doped yttrium lithium fluoride (Nd:YLF).

In this paper, a general characterization of the laser amplifier system is given in detail. In Section II, an overview of the laser system is presented. In Section III, a theoretical description of the laser is explained and the resultant equation for the steady-state and dynamic behavior is derived. In Section IV, the theory and the experimental data are compared. Summary of the results is presented in the concluding section.

II. Laser Scheme

The laser performance and characteristics are dictated by the basic parameters required by CTF3 as is seen from Table I. The 1.5-GHz micropulse structure specifies the choice of the mode-locked oscillator, the required electron bunch charge of 2.33 nC, and the quantum efficiency (QE) of 3% expected from Cs_2Te photocathode for a run of about 1 week, and fixes the UV micropulse energy (E_{UV}) and the wavelength to be, respectively, ~370 nJ and 262 nm. In order to satisfy such parameters, a continuous train of 8-ps micropulses arriving from the Nd:YLF oscillator and preamplifier (PA) (from High Q Laser Gmbh) at the fundamental 1047 nm wavelength is amplified by two powerful Nd:YLF multipass amplifiers, converted to the fourth harmonic at 262 nm, and delivered to the cathode. The intensity fluctuations must be below 0.1% rms, but a factor of 10 more (<1% rms) is acceptable for the initial feasibility tests. This stringent demand for the stability requires the laser to be run in a particular "steady-state" mode [11], [12], which will be referred to as SSS.

Manuscript received July 13, 2010; revised September 24, 2010; accepted October 1, 2010. Date of current version February 24, 2011. This work was supported in part by the PHIN photoinjector project, funded under the Joint Research Activity of CARE, which is the EU project for coordinated accelerator research in Europe, and has been built in collaboration among the Laboratoire de l'Accelerateur Linear, the Rutherford Appleton Laboratory, and the European Organization for Nuclear Research.

M. Petrarca and M. Divall are with the Engineering Department, Source Target and Interactions Group, European Organization for Nuclear Research, Geneva 23, Switzerland (e-mail: massimo.petrarca@cern.ch; marta.csatari@cern.ch).

M. Martyanov and G. Luchinin are with the Department of Nonlinear Dynamics and Optics, Institute of Applied Physics, Russian Academy of Science, Nizhny Novgorod 603950, Russia (e-mail: zebra-52@yandex.ru; luchining@appl.sci-nnov.ru).

Digital Object Identifier 10.1109/JQE.2010.2086047

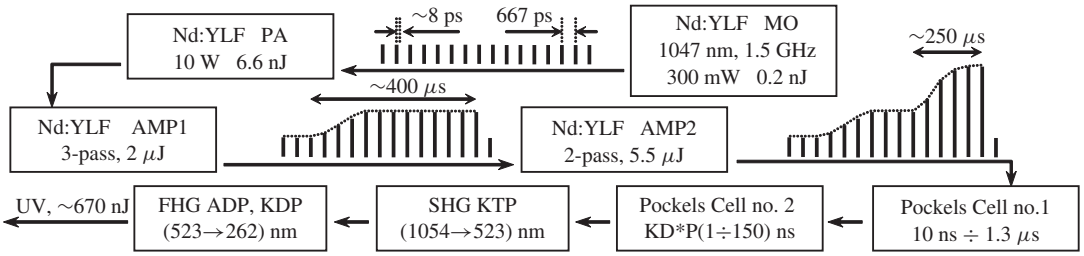

Fig. 1. Laser scheme.

TABLE I
MAIN PARAMETERS FOR TWO PHOTOINJECTORS WITH PARAMETERS NOT YET SATISFIED (HIGHLIGHTED)

			PHIN	CALIFES
Time structure	Bunch frequency, GHz		1.5	1.5
	Macropulse duration, ns		1272	0.01-150
	Bunches in macropulse		1907	NA
	Micropulse FWHM, ps	<	10	10
	Timing jitter, ps rms	<	1	1
	RR, Hz		5	5
Charge prod.	Charge/bunch, nC		2.33	0.6
	Charge stability, % rms	<	0.25 (0.1)	3
	Cs2Te : QE, %	>	3	0.3
	Wavelength, nm		262	262
Laser beam	UV energy / micropulse @ cathode, μJ		0.37	0.38 (0.95)
	IR-UV conversion efficiency	>	0.15	0.15 (0.2)
	Safe margin		0.55 (0.5)	0.7
	Laser beam transport transm.		0.82 (0.7)	0.64 (0.7)
	UV cath. energy / Output IR energy		0.07	0.076 (0.098)
	Output IR energy / micropulse, μJ		5.7	5.7 (10)
	Output IR macropulse mean power, kW		8.5	8.5 (15)

The steady-state mode permits implementing a time window with a high degree of intensity stability during which a $\sim 1.3-\mu$s long pulse may be selected. Hereinafter we will refer to this pulse with a substructure at 1.5 GHz as a "macropulse." The term "saturated" means that the mean input intensity is greater than the saturation intensity of the Nd:YLF, which reduces the response time needed for the amplifier to reach the stationary condition. The tight requirements to the intensity stability make pump diodes preferable to flash lamps. Moreover, implementation of a stabilizing feedback has been foreseen [15].

The overall fourth-harmonic conversion efficiency of $\sim 15\%$, additional transport losses, and safety margin to allow for the drop of the photocathode QE give a final conservative value of ~ 10 μJ for the infrared micropulse energy. To fulfill the CTF3 requirement to the PHIN photoinjector, a $\sim 1.3-\mu$s long macropulse is selected in the saturated part of the final amplification window and is passed to the frequency-conversion crystals. Only the first Pockels cell shown in Fig. 1, with rise and fall time of ~ 5 ns, is used for this purpose. For the CALIFES photoinjector, a combination of two Pockels cells is used to select just one single micropulse (gating width of ~ 1 ns) up to 150 ns window.

In this paper, we will focus our attention on the characteristics of two amplifiers and will omit details of the commercial master oscillator (MO) and PA produced by the company High Q Laser Production GmbH. A beam with a RR of 1.5 GHz and average output power of 10 W from the PA is transmitted through the first and the second Nd:YLF diode-pumped powerful amplifiers. The main parameters of the amplifier chain are listed in Table II. Both the amplifiers have a side-pumped rod configuration [16]. In order to increase the pump coupling efficiency, cylindrical lenses are placed in front of five diode stacks to focus the pumping beams into the rod [11], [12], [14]–[17] in the first amplifier (AMP1) and are removed from the second amplifier (AMP2) to pump the rod more homogeneously. AMP1 rod has a length of 80 mm, 70 mm of which is pumped, and a diameter of 7 mm pumped by 15 kW power for $\tau_1 = 400$ μs. AMP2 rod has a length of 120 mm (110 mm pumped) and a diameter of 10 mm pumped by 17.8 kW over $\tau_2 = 250$ μs. In order to reach high gain, a continuous pulse train from the PA is passed through AMP1 three times in a non-collinear configuration with a total propagation length of ~ 5 m, by which the un-amplified beam size at 4σ, changes from 3 to 4 mm. The amplified beam from AMP1 is then rotated to compensate for thermal lensing and an isolation system is installed to avoid feedback to the high-gain AMP1. AMP2 was originally designed to run in three passes, but steady-state is reached after two passes and a collinear double geometry provides the most efficient power extraction. A soft-aperture beam-shaping system was also proposed [8] (see Fig. 2). It is possible to produce a transverse (radial) beam profile proportional to $\cos^2(\pi/2(r/R)^2)$ (where $R = 4.9$ mm has been chosen to match the diameter of AMP2 rod). Unfortunately, the system itself introduces high losses of $\sim 80\%$ and cannot be used because AMP2 output power strongly depends on the input power. Consequently, the beam expander (BE) and the soft-edge polarization diaphragm (SD) depicted in Fig. 2 were replaced by a three-lens system. In this configuration, a Faraday rotator (FR) provides collinear geometry. The Nd:YLF crystal is cut in π-orientation in which only one polarization is amplified, supporting the 1047-nm line. Therefore, a $\lambda/2$ plate is used for convenience of alignment of the input polarization with the orientation of the YLF optical axis previously aligned vertically. By using the three-lens telescope mentioned above,

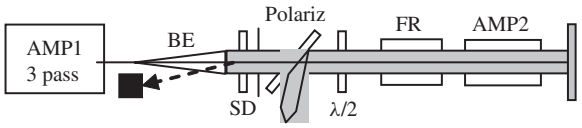

Fig. 2. AMP2 layout.

TABLE II
BASIC PARAMETERS OF THE BEAM IN A LASER CHAIN. VALUES EXPECTED FROM THE PROJECT [14]–[17] ARE LISTED IN THE LAST COLUMN

Output	**PA**	**AMP1**	**AMP2**	**AMP2** Project
P_m, kW	0.01	3	8.3	15
E_p, μJ	0.0066	2	5.5	10
G, gain		300 (6.7)	4.6 (2.14)	8.3
W_p / W_s		$\sim 1.4 \times 10^{-5}$	$\sim 8.1 \times 10^{-6}$	$\sim 1.4 \times 10^{-5}$
I_m / I_s		~ 10	~ 5.8	~ 10
τ_1, τ_2, μs		400	250	
P_{pump}, kW		15	17.8	

we explored different beam sizes and divergences in order to optimize the output power. Therefore, for utilizing as much stored energy as possible, the whole cross section of the rod must be exploited. The laser beam characteristics along the laser chain are shown schematically in Fig. 1 and a summary is given in Table II, where E_p is micropulse energy (also shown in Fig. 1), W_p is micropulse fluence, P_m is the mean macropulse power, I_m is mean macropulse intensity, $W_s = 1.1$ J/cm^2 is Nd:YLF saturation fluence, $\tau_r = 480$ μs is Nd:YLF radiative decay time, $I_s = W_s/\tau_r = 2.3$ kW/cm^2 is Nd:YLF saturation intensity [19], and G is the gain in the amplifiers (one pass gain is shown in brackets). It is worth nothing that parameters W_p/W_s and I_m/I_s are sensitive to beam shape, and the project parameters are estimated for a flat-top transverse beam distribution in two amplifiers: the selected diameter is 4 mm for AMP1 and 9 mm for AMP2.

The estimated average thermal power at 5-Hz operation is 6 W for the AMP1 and 7.8 W for the second. Thermal load per 1 cm rod length is close to 1 W/cm for both amplifiers, which is much less than the thermal fracture limit for an YLF crystal (15–17 W/cm) [19], [20]. As shown in [11], for our amplifiers which are under 15 W thermal load, the thermal lensing can be easily compensated by transport lenses, by rotating the beam between the two amplifiers, one can eliminate the astigmatism. But the thermal effects (fracture and lensing) will become the major concern in the future when this system will be upgraded to satisfy the upcoming CLIC parameters with a much higher average power at 50-Hz RR. This will be the issue of future studies and developments.

III. BASIC EQUATIONS AND OPERATING MODES

It is clear from the basic parameters listed in Table II what assumptions should be made in the analytical study, amplification of each individual micropulse occurs in a small-signal gain (SSG) mode, where each individual pulse passes through the active medium as a very weak signal ($W_p/W_s << 1$) and only slightly modifies the level of population inversion. This condition is valid even in the case of full-power operation. However, for macropulse amplification (a long train of micropulses) the amplification mode is strongly saturated ($I_m/I_s > 1$). This and the fact that the interval between the micropulses $T = 667$ ps (corresponding to the RR of 1.5 GHz) is much shorter than τ_r mean that the amplification in the steady-state can be considered to be the same as continuous wave (CW) amplification in the saturated mode. We will demonstrate how an expression for the behavior of this type of laser can be derived from the well-known Franz–Nodvik equations [19], [21], [22] for the amplification of micropulses and show the correlation between the formulated equation and the experimental data.

The amplification of one micropulse can be described by the Franz–Nodvik equations

$$\begin{cases} \dfrac{\partial I(t,z)}{\partial z} + \dfrac{1}{v}\dfrac{\partial I(t,z)}{\partial t} = K(t,z)I(t,z) & \text{(1a)} \\ \dfrac{\partial K(t,z)}{\partial t} = -\dfrac{I(t,z)}{W_s}K(t,z) + \text{Pump} - \text{Relaxation} & \text{(1b)} \end{cases}$$

where $I(t,z)$ is pulse intensity [W/cm^2], $K(t,z)$ is gain coefficient [cm^{-1}], and v is the velocity of light in the medium.

In our case, it can be assumed that the pump power that is applied to the amplifier has a constant value over the pumping window. Therefore, the term "Pump" in (1b) may be written as

$$\text{Pump} = \frac{K_0}{\tau_r} = \frac{\ln G_0}{(L\tau_r)} \tag{2}$$

where $G_0 = \exp(K_0 L)$ is the theoretical single-pass SSG of the amplifier when the amplified spontaneous emission (ASE) contribution is neglected and K_0 indirectly describes the pump power delivered to the laser transition; saturation of the pump transition has been ignored. The pump saturation effect (depletion of ground state in a four-level system) in the case of SSG mode with a large value of G may be neglected. The neodymium concentration for 1% doping level is estimated to be $N_{Nd} = 1.4 \times 10^{20}$ cm^{-3}, the concentration of excited Nd atoms $N^* = (\ln G)/(\sigma L)$, where $\sigma = 1.8 \times 10^{-19}$ cm^2 is the lasing cross section and $L = 10$ cm is the rod length. Calculations for $G = 1000$, which is of the order of magnitude of the measured G_0 (see Section IV-B), yield $N^* = 3.8 \times 10^{18}$ cm^{-3}. Therefore, the ratio $N^*/N_{Nd} = 0.027$ is much less than unity, which supports the validity of the assumption.

For convenience, the following expression has been chosen for the relaxation term:

$$\text{Relaxation} = \frac{K(1 + A(K))}{\tau_r} \tag{3}$$

where $A(K)$ is the ASE contribution, which is zero in the simplest case. For description of the pump effect on the rod when no input signal is present and the ASE contribution is neglected, (1) can be simplified as follows:

$$\frac{\partial K(t,z)}{\partial t} = \frac{K_0 - K(t,z)}{\tau_r} \tag{4}$$

with the solution $K(t,z) = K_0(1 - e^{-t/\tau_r})$, where $K(t = 0, z) = 0$. From this, K_0 (and the related parameter $G_0 = e^{K_0 L}$) can be defined as the gain coefficient achieved by the medium over infinite time ($t >> \tau_r$) neglecting ASE.

Inserting (3)–(5) into (1) yields a coupled equation for micropulse amplification

$$\begin{cases} \dfrac{\partial I(t,z)}{\partial z} + \dfrac{1}{v}\dfrac{\partial I(t,z)}{\partial t} = K(t,z)I(t,z) \\ \dfrac{\partial K(t,z)}{\partial t} = -\dfrac{K(t,z)I(t,z)}{W_s} + \dfrac{K_0 - K(t,z)(1+A(K))}{\tau_r}. \end{cases} \tag{5}$$

The micropulse duration of 8 ps and the period between micropulses $T = 667$ ps are very short compared to the fluorescence lifetime $\tau_r = 480\ \mu$s. Therefore, the gain $K(t,z)$ at each point of the rod will have a smooth time-dependent behavior under pump and relaxation processes and will slightly change when the micropulse passes through a certain point. The smooth behavior of $K(t, z)$ is obtained by averaging (5) over the period T.

Let $K^*(t,z) = \frac{1}{T}\int_t^{t+T} K(t,z)dt$ be the smooth gain we are interested in, and let $W_p(t,z) = \int_t^{t+T} I(t,z)dt$ be fluence. Hereafter, we will omit $A(K)$ for simplicity and will take ASE into consideration in the final expression. Then, the system of coupled equations (5), after some mathematical manipulations and integration over the length of the medium, takes on the form

$$\begin{cases} W_p(t,L) - W_p(t,0) = \int_0^L K^*(t,z)W_p(t,z)dz \\ \frac{\partial \ln G}{\partial t} = -\frac{1}{TW_s}\int_0^L K^*(t,z)W_p(t,z)dz + \frac{1}{\tau_r}(\ln G_0 - \ln G) \end{cases} \tag{6}$$

where $G(t) = \exp\left(\int_0^L K(t,z)dz\right)$ is the single-pass gain.

By substituting the integral from the first equation into the second and using the fact that $W_p(t,L) = G(t)\ W_p(t,0)$, we obtain the following equation:

$$\frac{\partial \ln G(t)}{\partial t} = -\frac{W_p(t,0)}{W_s}\frac{G(t)-1}{T} + \frac{\ln G_0 - \ln G(t)}{\tau_r}. \tag{7}$$

For the mean intensity, defined as $I_m = W_p/T$, and saturation intensity $I_s = W_s/\tau_r$, (7) can be rewritten in the form

$$\tau_r\frac{\partial \ln G(t)}{\partial t} = -\frac{I_m(t,0)}{I_s}(G(t)-1) + \ln G_0 - \ln G(t). \tag{8}$$

In the case of the one-pass scheme, this equation can be considered as an intensity balance law. In fact, with allowance for the spontaneous emission intensity losses $I_L = W_{st}/\tau_r$, the pump intensity $I_p = I_s \ln G_0$ and the extracted intensity $\Delta I = I_m(t,0)(G-1)$ (8) can be rewritten in the form

$$\frac{\partial W_{st}}{\partial t} = -\Delta I + I_p - I_L \tag{8a}$$

which shows time variation of the storage fluence.

In the case of N passes with total gain $G = G_1^N$ (G_1 is one-pass gain), the intensity balance law will be the same but the definition of stored energy has to be changed to $E = W_s \ln G_1 = W_s \ln G/N$. Therefore, in the case of the N-pass scheme where G is the total gain for N passes, (8) takes on the form

$$\frac{\tau_r}{N}\frac{\partial \ln G(t)}{\partial t} = -\frac{I_m(t,0)}{I_s}(G(t)-1) + \ln G_0 - \frac{\ln G(t)}{N}. \tag{9}$$

This simple modification is possible when, as in our case, the overlapping of two micropulses is small enough (1.6 mm for an 8-ps pulse) compared to the rod length L and its effect on the amplifier gain can be neglected.

In order to include ASE, we modify this equation as is done in [15]

$$\frac{\tau_r}{N}\frac{\partial \ln G}{\partial t} = -\frac{I_m(t,0)}{I_s}(G-1) + \ln G_0 - \frac{\ln G}{N}(1+B(G)) \tag{10}$$

where $B(G)$ is the integrated $A(K)$ ASE contribution, including coupling between the passes [19].

The stationary solution of this equation is the well-known steady-state mode

$$\frac{I_m^{(in)}}{I_s} = \left[\frac{\ln G_0 - \frac{\ln G}{N}(1+B(G))}{(G-1)}\right] \tag{11}$$

where $I_m^{(in)}$ is input intensity. In the steady-state operation, one micropulse passes through the rod and acquires a small portion of the energy stored in the medium, another small portion of this energy is taken by the relaxation process, and up to the next pulse the pump refills this decrease of energy up to the value of the initial state. The balance of these three processes is described by (11).

In the case of N-pass scheme, if we neglect feedback between the passes, B depends only on the one-pass gain $G_1 = \sqrt[N]{G}$, and $B = B(G_1)$. Otherwise, if there is feedback from one pass to another, the coupling parameter has to be determined. In Section IV-B, we will discuss this issue by fitting the measured values with power law.

Following [15], by differentiating (11) with $I_{out} = GI_{in}$ it is possible to estimate relative sensitivity of the system

$$\frac{\delta I_{out}/I_{out}}{\delta I_{in}/I_{in}} = \frac{dI_{out}}{dI_{in}}\frac{I_{in}}{I_{out}} = \frac{dI_{out}}{dI_{in}}\frac{1}{G} = 0.265 \sim \frac{1}{G}$$

$$\frac{dI_{out}}{dI_{in}} = \frac{(G-1) + 2\ln G_0 - \ln G}{(1-1/G) + 2\ln G_0 - \ln G} = 1.22$$

where we assume $I_{in} = 1.8$ kW, $I_{out} = 8.3$ kW, and $G_0 = 863$, which gives $G = 4.6$. Thus, the stability of the system in the SSS mode is inversely proportional to the total gain [15]. Therefore, in this case a chain of high-gain amplifiers provides a good shot-to-shot stability of the system in combination with the intrinsic stability of pumping diode and input seed.

The SSS condition ensures good stability along the selected macropulse. Stability of the IR and UV shot-to-shot intensity has been measured, respectively, by placing a Gentec joule meter just after the Pockels cell and after the fourth-harmonic-generation crystal. The macropulse length required by PHIN has been selected for measurements. A rms of ~0.4% for IR and of ~1.3% for UV has been measured over a 500-shot statistics. A shot-to-shot measurement of the electron beam current produced by the generated ~1.3-μs electron macropulse [10] showed a rms value in agreement with the one measured directly on the UV laser beam. The electron beam current measurement has been performed during the PHIN runs using a standard device called "beam position monitor" for particle beam diagnostics described in [23].

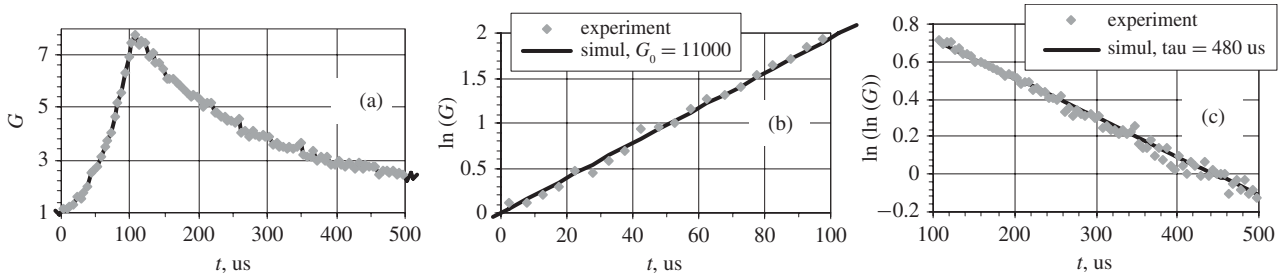

Fig. 3. (a) AMP1 SSG measurement. (b) Amplification (11). (c) Relaxation (12).

IV. Amplifiers Characterization

A. AMP1

SSG measurements were performed to characterize the AMP1. Toward this end, the pumping time was reduced down to $\tau_1 = 100\ \mu$s and the input power to 200 mW. The relaxation behavior was observed for 400 μs after switching off the pump. As the 4σ beam diameter was ~3 mm, the intensity was still small enough compared to the Nd:YLF saturation intensity (2.3 kW/cm^2) to ensure the SSG regime. A G_1 value close to 8 has been measured (output power 1.6 W). In this mode, we obtained good correlation between the measurements reported in Fig. 3(a) and the simulations, in which the first term in (1b) with respect to the pump was neglected and also the third term was omitted because the pumping time was set to be $\tau_1 < \tau_r = 480\ \mu$s.

In this way, equations of the system (1) become uncoupled and we can integrate the simplified version of the second equation. During the pumping time, it has the form

$$\ln G = \frac{(\ln G_0)t}{\tau_r} \qquad \text{for } 0 \le t \le \tau_1. \tag{12}$$

In Fig. 3(b), (12) is represented by the solid curve, and the measured data by the dots, the slope of the curve gives the value for fitting parameter $G_0 = 11\ 000$. The SSG mode is corroborated by the agreement between the measured data in Fig. 3(c) [sloping-down part of the curve in Fig. 3(a)] and the simulation for the relaxation time. From (1b) by setting $G_0 = 1$ and neglecting ASE and the first term (at least for the beginning of the decay), we obtain

$$\ln \ln G = \frac{(\tau_1 - t)}{\tau_r} + \ln \ln G(\tau_1) \qquad \text{for } t \ge \tau_1. \tag{13}$$

Good agreement between (13) with $\tau_r = 480\ \mu$s (solid line) and the measured data (dots) plotted in Fig. 3(c) corroborates the assumptions made.

B. AMP2: SG and ASE

To perform the SSG measurements, the diode pump duration was increased up to 1400 μs (instead of 250 μs in normal operating conditions). The key point was to create a situation when the SSG acquires a steady-state ($t > \tau_r$). This steady-state gain must not be confused with the SSS which is established during normal operation when $t < \tau_r$ and $I_m/I_s > 1$, although they have the same origin, the balance between all the processes.

The steady-state here is the result of the balance between the absorbed pump power and the losses due to spontaneous emission and ASE only, as the extraction is negligible. Equation (7) was modified to

$$\tau_r \frac{\partial \ln G(t)}{\partial t} = \ln G_0 - \ln G(t)\ (1 + B(G)). \tag{14}$$

Thereafter, by considering that $G(t)$ does not depend on transverse coordinates, the initial condition is $G(t = 0) = 1$, and neglecting the ASE ($B = 0$), the solution of (14) is found to be

$$\ln G(t) = \ln G_0 \left(1 - e^{\frac{-t}{\tau_r}}\right) \tag{15}$$

where behavior of the curve depends only on one fitting parameter G_0. Note that $G(t)$ tends to the constant G_0 when $t >> \tau_r$.

Comparison of the experiment and the simulation curves is shown in Fig. 4, where one can see that, by neglecting the ASE (dashed curve) from the simulation, a good agreement in the time interval $0 < t < 500\ \mu$s (corresponding to the gain interval $1 < G < 100$) is found, the fitted value from this part of the curve for G_0 is 863. This G_0 value leads to the maximum intensity that one can extract from the rod in a 10-mm flat-top beam (the maximum parameters of the setup), $I_{lim} = I_s \ln G_0 = 15.5$ kW/cm^2 and $P_{lim} = I_{lim} S = 12.2$ kW. This power can be extracted only in the case of a very strong input signal, i.e., when the required gain is small. Compare the value of P_{lim} with the estimated power absorbed from the pumping diodes. The power emitted from one diode bar driven by 90-A current is 81 W (from DiLas calibration diode curve), the AMP2 consists of 5×44 bars, so the total emitted pumping power of AMP2 is 17.8 kW. The maximum pump-to-optical efficiency in AMP2 is therefore 12.2 kW/17.8 kW = 0.68.

It is clear from Fig. 4 that the experimentally achieved gain (grey curve) is much less than that without taking ASE into consideration (dashed curve). From this we can conclude that the ASE contribution becomes important when the gain is over 100. We tried different ASE models available in the literature [11], [15], [24], these models include the dependence on the geometry (diameter to length ratio), but they do not fit our case.

In order to get a phenomenological expression, which in our case can take into account the ASE contribution, we tried polynomials of different orders. We found the best fit by using a simple power law depending on two parameters a and b

$$B = aG^b. \tag{16}$$

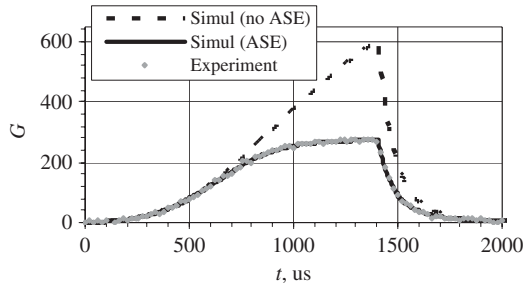

Fig. 4. SSG measurement for AMP2. Dashed black curve is the simulation neglecting ASE and the solid black curve is including ASE, dotted grey curve is the experimental data.

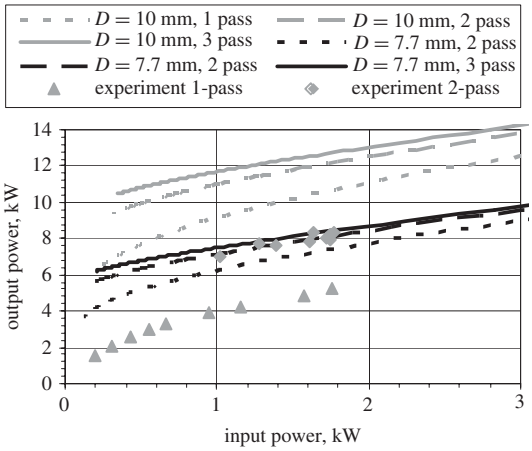

Fig. 5. AMP2 output power versus input power for one-, two-, and three-pass system in the steady-state mode for two different beam diameters $D = 10$ mm and 7.7 mm.

The best fit was obtained with $a = 2.7 \times 10^{-6}$ and $b = 2$ (see the solid curve in Fig. 4). In this way, we have fully characterized the system, even though the physical meaning and the dependence on the rod geometry of parameters a and b is not clear. Formal description of these parameters may be the issue of further studies. But even now we can use this particular ASE model for this particular amplifier to improve its performance in different modes.

C. AMP2: Full-Power Steady-State Operation

Summarizing the results of the previous section, we can say that for 250 μs pump duration and single pass gain not higher than 4, the ASE contribution can be neglected, i.e., $B = 0$. This has also been verified by measurements of the two-pass gain, which agrees with G_1^2, as is to be expected neglecting ASE, and the one-pass gain is G_1. It is therefore possible to rewrite (10) in the form

$$I^{in} = I_s \left(\frac{\ln G_0 - \frac{\ln G}{N}}{(G-1)} \right). \tag{17}$$

Using $I^{out} = GI^{in}$ and $I_{\lim} = I_s \ln G_0$ we can plot the output intensity I_{out} versus the input intensity I_{in} in AMP2 for $G_0 = 863$ obtained in the SSG measurements and beam diameter 10 mm (flat-top beam fully filling the rod, the maximum parameters of the setup). The curves of the output

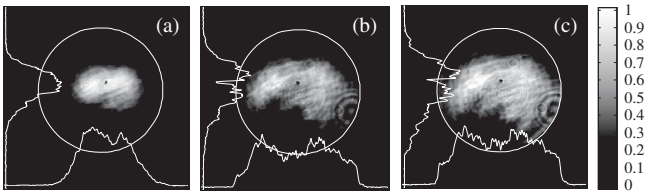

Fig. 6. Image plane corresponding to the end of the first passage along the rod of AMP2 in three different situations. (a) Non-amplified beam (AMP1, 2 off), $F = 0.17$. (b) Amplified by AMP1 at full power (AMP2 off), $F = 0.28$. (c) Amplified by AMP1 and AMP2 at full power, $F = 0.38$. The white circle delimits the rod diameter of 10 mm.

versus input power are plotted in Fig. 5 for one-, two-, and three-pass systems in the steady-state mode. Using a three-pass system instead of a two-pass system will not give a significant gain in output power, but will complicate the setup. Fig. 5 also shows that in the two-pass scheme in the ideal case of a flat-top beam with a diameter of 10 mm, the output power cannot exceed 13.5 kW for a 3-kW seed (AMP1 output currently available) and 12 kW for a 1.7-kW seed (that is the AMP2 input because of the losses along the beam transport line between AMP2 and AMP1). In Fig. 5, the black curves show the output versus input power for a flat-top beam 7.7 mm in diameter, and in this case $P_{lim} = 7.2$ kW. This diameter was chosen to match the experimental data (diamonds). As suggested also by Fig. 5, there are two ways to increase the output power. The first one is to decrease losses on the beam transport line between the two amplifiers, thus increasing the output power from 8.3 to 9.5 kW. The second possibility is to increase the interaction volume of the propagating beam within the AMP2 rod (increasing the fill factor). With this strategy, the output power can be increased from 8.3 up to 12 kW, and, if the losses along the beam line between the amplifiers are reduced, the highest achievable output power can reach the value of 13.5 kW.

The necessity to increase the beam diameter and to fill the rod better is also apparent from Fig. 6, where the beam cross section of the image plane corresponding to the end of the first passage along the rod of AMP2 is shown for three different situations: (a) non-amplified beam (AMP1 off) with fill factor 0.17; (b) amplified by AMP1 at full power (AMP2 off) with fill factor 0.28; and (c) amplified by AMP1 and AMP2 at full power with fill factor 0.38. The transverse beam profile has to be increased to fill up all the volume of the rod whose edges are clearly visible and can be used as a reference for the dimension of the beam. From Fig. 6, it is also clear that the beam profile should be improved to reduce its ellipticity and clipping. The beam profile improvement will be the objective of future work.

The case of a single passage through the AMP2 during normal operation has also been plotted in Fig. 5 for completeness (triangles). Since the saturation is not reached in a single passage, it is natural that the experimental results do not agree with the theoretical curve following from (17).

D. AMP2: Full Power Dynamics

Measurements of the AMP2 characteristics in one-pass and two-pass schemes were carried out under normal operating

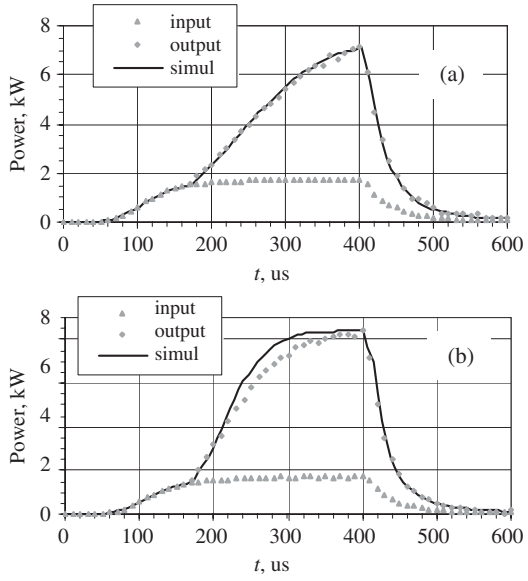

Fig. 7. Comparison of experimental data and simulation of amplification dynamics in the case of (a) single passage and (b) double passage through AMP2.

conditions, i.e., the pump duration of AMP1 and AMP2 was set to be 400 μnd 250 μs, respectively. Numerical simulation was compared with results of experiment, see Fig. 7(a) and (b). During normal operation $I_m/I_s > 1$, therefore, the amplifiers are saturated, which means that there is a strong depletion of the stored energy in the rod and the steady-state is reached in time $t < \tau_r$. It should be emphasized that the really important parameter that must be considered is the intensity, which depends on the beam transverse distribution (flat-top, Gaussian, etc.). However, it is not straightforward to make simulations allowing for the real transverse beam profile propagating through the rod, as it is modified by the amplification process and by the thermal properties of the rod. Therefore, a different simpler approach with a 7.7-mm flat-top beam corresponding to the experimental data (see Section IV-C) was used.

For a nonideal beam with nonuniform transverse distribution, a steady-state is reached first for the highest intensity (central area of the beam) and then for the wings of the beam. Due to the experimental transverse distribution, the total power of the beam behaves differently with respect to a flat-top beam. This discrepancy is readily seen in Fig. 7(b), the flat-top beam attains the steady-state faster than the experimental beam with nonuniform transverse intensity distribution. In Fig. 7(a) and (b), even though the transverse beam distribution has not been taken into account along its propagation through AMP2, it is possible to see a satisfactory agreement between the simulation and the experiments in the case of one and two passages, respectively. It should be pointed out that the experimental data have been acquired using a photodiode with an active area larger than the beam diameter. Consequently, the whole beam has been detected. The output signal from the photodiode is therefore an integrated result over the beam profile and gives an average value of the temporal behavior for different parts of the beam.

Equation (9) for the dynamic behavior of the laser was derived from the Franz–Nodvik equations. Besides, a step-by-step code based on (1) was written in MATLAB. Simulation of the code (not shown here) also corroborated the validity of (9).

V. Conclusion

In this paper, we have characterized the behavior of the CTF3 photoinjector laser system, showing that the amplification dynamics can be found from the Frantz–Nodvik equation for the micropulse amplification mode. We have shown that each single micropulse weakly affects amplifier gain by carrying a fluence well below the saturation fluence of the active material, even for the nominal value of the amplified micropulse. We have demonstrated satisfactory agreement between the experimental data and results of the simulation.

We have shown that the amplifiers behave like CW amplifiers. Due to the high input intensity, the time necessary to reach steady-state decreases compared to the situation when the input intensity is lower than the saturation intensity. We have shown that the laser has a good intrinsic intensity stability of $\sim$0.4% rms in the infrared and $\sim$1.3% rms in the UV region.

The laser in its present configuration is used daily to drive successfully the two CTF3 photoinjector lines. Improvements of the laser system are under way, aiming at reaching all the project requirements.

VI. Acknowledgment

The Laboratoire de l'Accelerateur Linear is responsible for the design and construction of the RF gun [25], the Rutherford Appleton Laboratory and the European Organization for Nuclear Research (CERN) for the design and construction of the laser, and CERN for producing the photocathodes, overall coordination, and commissioning. The authors would like to thank V. Fedosseev, CERN, E. Khazanov, Institute of Applied Physics, Russian Academy of Science (IAP, RAS), A. Poteomkin, IAP, RAS, and V. Lozkharev, IAP, RAS, for collaboration and helpful discussions. They also thank N. Lebas, CERN, for technical support, and the PHIN Photoinjector Group for the electron beam current stability measurements.

References

[1] G. Geschonke and A. Ghigo, "CTF3 design report," Eur. Org. Nucl. Res. (CERN), Geneva, Switzerland, Rep. CERN-PS-2002-008-RF; CTF-3-NOTE-2002-047; LNF-2002-008-IR, May 24, 2002.

[2] H. Braun, R. Corsini, J.-P. Delahaye, A. De Roeck, S. Doebert, G. Geschonke, A. Grudiev, C. Hauviller, B. Jeanneret, E. Jensen, T. Lefevre, Y. Papaphilippou, G. Riddone, L. Rinolfi, W.-D. Schlatter, H. Schmickler, D. Schulte, I. Syratchev, M. Taborelli, F. Tecker, R. Tomás, S. Weisz, and W. Wunsch, "CLIC 2008 parameters," Eur. Org. Nucl. Res., Geneva, Switzerland, Rep. CLIC-NOTE-764, 2008.

[3] G. Geschonke, "Results from the CLIC test facility CTF3 and update on the CLIC design," in *Proc. EPAC*, Genoa, Italy, 2008, pp. 2912–2916.

[4] H. H. Braun, E. Chevallay, S. Hutchins, P. Legros, G. Suberlucq, H. Trautner, I. N. Ross, and E. Bente, "The photo-injector option for CLIC: Past experiments and future developments," in *Proc. PAC*, Chicago, IL, Jun. 2001, pp. 720–722.

[5] M. Reiser, *Theory and Design of Charge Particle Beams*. New York: Wiley, 1994.

[6] C. A. Brau, *What Brightness Means, in Physics of High Brightness Beams*. Singapore: World Scientific, 2003.
[7] H. H. Braun, R. Corsini, A. De Roeck, A. Grudiev, S. T. Heikkinen, E. Jensen, M. S. Korostelev, D. Schulte, I. V. Syratchev, F. A. Tecker, W. Wuensch, and F. Zimmermann, "Updated CLIC parameters," Eur. Org. Nucl. Res., Geneva, Switzerland, Rep. CLIC-NOTE-627, CERN-OPEN-2006-022, 2006.
[8] M. Petrarca, H. H. Braun, E. Chevallay, S. Doebert, K. Elsener, V. Fedosseev, G. Geschonke, R. Losito, A. Masi, O. Mete, L. Rinolfi, A. Dabrowski, M. Divall, N. Champault, G. Bienvenu, M. Jore, B. M. Mercier, C. Prevost, R. Roux, and C. Vicario, "First results from commissioning of the PHIN photo injector for CTF3," in *Proc. PAC*, Vancouver, BC, Canada, 2009, pp. 1–3.
[9] R. Losito, H. H. Braun, N. Champault, E. Chevallay, V. Fedosseev, A. Kumar, A. Masi, G. Suberlucq, M. Divall, G. Hirst, G. Kurdi, W. Martin, I. Musgrave, I. Ross, E. Springate, G. Bienvenu, B. Mercier, C. Prevost, and R. Roux, "The PHIN photoinjector for the CTF3 drive beam," in *Proc. EPAC*, Edinburgh, Scotland, 2006, pp. 1–3.
[10] M. Petrarca, E. Chevallay, S. Doebert, A. Dabrowski, M. Divall, V. Fedosseev, N. Leabas, T. Lefevre, and R. Losito, "Performance of the PHIN high charge photo injector," in *Proc. IPAC*, Kyoto, Japan, 2010, pp. 4122–4124.
[11] I. N. Ross, M. Csatári, and S. Hutchins, "High-performance diode-pumped Nd:YLF amplifier," *Appl. Opt.*, vol. 42, no. 6, pp. 1040–1047, Feb. 2003.
[12] M. Divall, G. Kurdi, I. Musgrave, E. Springate, W. Martin, G. J. Hirst, and I. N. Ross, "Design and testing of amplifiers for the CTF3 photo-injector laser," Eur. Org. Nucl. Res., CARE, Geneva, Switzerland, Rep. 06-021-PHIN, 2006.
[13] I. Will, "Optical laser syncronized to the DESY VUV-FEL for two-color pump-probe experiments," in *Proc. 27th Int. Free Electron Laser Conf.*, Stanford, CA, Aug. 2005, pp. 690–693.
[14] Y. Tang, M. Divall, I. N. Ross, E. Springate, and G. J. Hirst, "High power diode-pumped Nd:YLF amplifier development," Rutherford Appleton Lab., Central Laser Facility, Didcot, U.K., Annu. Rep. 2004/2005.
[15] I. N. Ross, "Feasibility study for the CERN 'CLIC' photo-injector laser system," CERN, Geneva, Switzerland, Tech. Rep. CLIC-NOTE-462, 2000.
[16] I. Ross and S. J. Hutchins, "A laser system design for the photo-injector option for the CERN linear collider," Rutherford Appleton Lab., Central Laser Facility, Didcot, U.K., Annu. Rep. 2000/2001.
[17] G. Kurdi, I. O. Musgrave, M. Divall, E. Springate, W. Martin, G. J. Hirst, and I. N. Ross, "Development of the CTF3 photo-injector laser system," Rutherford Appleton Lab., Central Laser Facility, Didcot, U.K., Annu. Rep. 2006/2007.
[18] M. A. Martyanov, A. K. Poteomkin, A. A. Shaykin, and E. A. Khazanov, "Formation of a beam profile at the input to a high-energy laser amplifier," *Quantum Electron.*, vol. 38, no. 4, pp. 354–358, 2008.
[19] W. T. Silfvast, *Laser Fundamentals*. Cambridge, U.K.: Cambridge Univ. Press, 2000.
[20] G. Cerullo, S. De Silvestri, and V. Magni, "High efficiency, 40 W CW Nd:YLF laser with large TEM_{00} mode," *Opt. Commun.*, vol. 93, nos. 1–2, pp. 77–81, Sep. 1992.
[21] L. M. Frantz and J. S. Nodvik, "Theory of pulse propagation in a laser amplifier," *J. Appl. Phys.*, vol. 34, no. 8, pp. 2346–2349, 1963.
[22] A. E. Siegman, *Lasers*. Mill Valley, CA: University Science, 1986.
[23] D. Brandt, "Foreword," in *Proc. CERN Accel. School: Course Beam Diagnostics*, Dourdan, France, May–Jun. 2008, p. 598.
[24] S. B. Papernyĭ, V. A. Serebryakov, and V. E. Yashin, "Formation of a smooth transverse distribution of intensity in a light beam by a phase-rotating plate," *Sov. J. Quantum Electron.*, vol. 8, no. 9, pp. 1165–1166, 1978.
[25] R. Roux, "Conception of photo-injectors for the CTF3 experiment," *Int. J. Modern Phys. A*, vol. 22, no. 22, pp. 3925–3941, 2007.

Massimo Petrarca was born in Rome, Italy, on January 3, 1981. He received the Masters and Ph.D. degrees in physics from the Sapienza University of Rome, Rome, in 2003 and 2008, respectively. His doctoral dissertation involved studies on photoinjector laser systems and laser pulse shaping techniques.

He has been a Senior Fellow at the European Organization for Nuclear Research, Geneva, Switzerland, carrying out post-doctoral research on high power photoinjector lasers, photo cathodes, and photoinjector optimizations, since 2008. His current research interests include ultrafast optics, solid-state lasers, laser pulse shaping, diagnostics, and nonlinear optics.

Mikhail Martyanov was born in Nizhny Novgorod (formerly Gorky), Russia, in 1979. He received the M.S. degree in physics from the Nizhny Novgorod State University, Nizhny Novgorod, in 2002. He is currently working toward the Ph.D. degree at the Institute of Applied Physics, Russian Academy of Sciences, Nizhny Novgorod.

His current research interests include solid-state lasers and nonlinear optics.

Marta "Csatari" Divall was born in Berettyoujfalu, Hungary, in 1977. She received the M.S. degree in physics and mathematics from the University of Szeged, Szeged, Hungary, in 2000. During her postgraduate study, she investigated loss processes in nonlinear cystals and temporal contrast of ultrashort laser pulses.

She was with Rutherford Appleton Laboratory, Science and Technology Facilities Council, Didcot, U.K., as a Visiting Scientist from 2001 to 2005, on diode-pumped solid-state laser development for photoinjector and optical parametric chirped-pulse amplification pump laser applications. Since 2009, she has been with the European Organization for Nuclear Research, Geneva, Switzerland, as a Senior Fellow, continuing research on the development of photoinjector lasers. Her current research interests include solid-state lasers, nonlinear optics, and temporal contrast.

Grigory Luchinin was born in Nizhny Novgorod (formerly Gorky), Russia, in 1972. He received the M.S. degree in physics from the Nizhny Novgorod State University, Nizhny Novgorod, in 1994.

He is currently working as a Senior Researcher at the Institute of Applied Physics, Russian Academy of Science, Nizhny Novgorod. His current research interests include solid-state lasers and nonlinear optics.